

## Nuclear Stopping in Au + Au Collisions at $\sqrt{s_{NN}} = 200$ GeV

I. G. Bearden,<sup>7</sup> D. Beavis,<sup>1</sup> C. Besliu,<sup>10</sup> B. Budick,<sup>6</sup> H. Bøggild,<sup>7</sup> C. Chasman,<sup>1</sup> C. H. Christensen,<sup>7</sup> P. Christiansen,<sup>7</sup> J. Cibor,<sup>3</sup> R. Debye,<sup>1</sup> E. Enger,<sup>12</sup> J. J. Gaardhøje,<sup>7</sup> M. Germinario,<sup>7</sup> K. Hagel,<sup>8</sup> O. Hansen,<sup>7</sup> A. Holm,<sup>7</sup> A. K. Holme,<sup>12</sup> H. Ito,<sup>11,1</sup> A. Jipa,<sup>10</sup> F. Jundt,<sup>2</sup> J. I. Jørdre,<sup>9</sup> C. E. Jørgensen,<sup>7</sup> R. Karabowicz,<sup>4</sup> E. J. Kim,<sup>1,11</sup> T. Kozik,<sup>4</sup> T. M. Larsen,<sup>12</sup> J. H. Lee,<sup>1</sup> Y. K. Lee,<sup>5</sup> G. Løvholden,<sup>12</sup> Z. Majka,<sup>4</sup> A. Makeev,<sup>8</sup> M. Mikelsen,<sup>12</sup> M. Murray,<sup>8,11</sup> J. Natowitz,<sup>8</sup> B. S. Nielsen,<sup>7</sup> J. Norris,<sup>11</sup> K. Olchanski,<sup>1</sup> D. Ouerdane,<sup>7</sup> R. Płaneta,<sup>4</sup> F. Rami,<sup>2</sup> C. Ristea,<sup>10</sup> D. Röhrich,<sup>9</sup> B. H. Samset,<sup>12</sup> D. Sandberg,<sup>7</sup> S. J. Sanders,<sup>11</sup> R. A. Scheetz,<sup>1</sup> P. Staszal,<sup>7,4</sup> T. S. Tveter,<sup>12</sup> F. Videbæk,<sup>1</sup> R. Wada,<sup>8</sup> Z. Yin,<sup>9</sup> and I. S. Zgura<sup>10</sup>

(BRAHMS Collaboration)

<sup>1</sup>Brookhaven National Laboratory, Upton, New York 11973

<sup>2</sup>Institut de Recherches Subatomiques and Université Louis Pasteur, Strasbourg, France

<sup>3</sup>Institute of Nuclear Physics, Krakow, Poland

<sup>4</sup>Smoluchowski Institute of Physics, Jagiellonian University, Krakow, Poland

<sup>5</sup>Johns Hopkins University, Baltimore, Maryland 21218, USA

<sup>6</sup>New York University, New York, New York 10003, USA

<sup>7</sup>Niels Bohr Institute, Blegdamsvej 17, University of Copenhagen, Copenhagen 2100, Denmark

<sup>8</sup>Texas A&M University, College Station, Texas 77843, USA

<sup>9</sup>Department of Physics, University of Bergen, Bergen, Norway

<sup>10</sup>University of Bucharest, Bucharest, Romania

<sup>11</sup>University of Kansas, Lawrence, Kansas 66045, USA

<sup>12</sup>Department of Physics, University of Oslo, Oslo, Norway

(Received 31 December 2003; published 30 August 2004)

Transverse momentum spectra and rapidity densities,  $dN/dy$ , of protons, antiprotons, and net protons ( $p - \bar{p}$ ) from central (0%–5%) Au + Au collisions at  $\sqrt{s_{NN}} = 200$  GeV were measured with the BRAHMS experiment within the rapidity range  $0 \leq y \leq 3$ . The proton and antiproton  $dN/dy$  decrease from midrapidity to  $y = 3$ . The net-proton yield is roughly constant for  $y < 1$  at  $dN/dy \sim 7$ , and increases to  $dN/dy \sim 12$  at  $y \sim 3$ . The data show that collisions at this energy exhibit a high degree of transparency and that the linear scaling of rapidity loss with rapidity observed at lower energies is broken. The energy loss per participant nucleon is estimated to be  $73 \pm 6$  GeV.

DOI: 10.1103/PhysRevLett.93.102301

PACS numbers: 25.75.Dw

The energy loss of colliding nuclei is a fundamental quantity determining the energy available for particle production (excitation) in heavy ion collisions. This deposited energy is essential for the possible formation of a deconfined quark-gluon phase (QGP) of matter. Because the baryon number is conserved, and rapidity distributions are only slightly affected by rescattering in late stages of the collision, the measured net-baryon ( $B - \bar{B}$ ) distribution retains information about the energy loss and allows the degree of nuclear stopping to be determined. Such measurements can also distinguish between different proposed phenomenological mechanisms of initial coherent multiple interactions and baryon transport [1–3].

The average rapidity loss,  $\langle \delta y \rangle = y_p - \langle y \rangle$  [4], is used to quantify stopping in heavy ion collisions [5,6]. Here,  $y_p$  is rapidity of the incoming projectile and  $\langle y \rangle$  is the mean net-baryon rapidity after the collision:

$$\langle y \rangle = \frac{2}{N_{\text{part}}} \int_0^{y_p} y \frac{dN_{(B-\bar{B})}(y)}{dy} dy, \quad (1)$$

where  $N_{\text{part}}$  is the number of participating nucleons in the collision. The two extremes correspond to full stopping, where initial baryons lose all kinetic energy ( $\langle \delta y \rangle = y_p$ ), and full transparency, where they lose no kinetic energy ( $\langle \delta y \rangle = 0$ ). For fixed collision geometry (system size and centrality) at lower energy [Schwer Ionen Synchrotron (SIS), Alternating Gradient Synchrotron (AGS), and Super Proton Synchrotron (SPS)] it was observed that  $\langle \delta y \rangle$  is proportional to the projectile rapidity. For central collisions between heavy nuclei (Pb, Au),  $\langle \delta y \rangle \sim 0.58 y_p$  [6–8].

Bjorken assumed that sufficiently high energy collisions are “transparent”; thus the midrapidity region is approximately net-baryon-free [9]. The energy density early in the collision,  $\epsilon$ , can then be related in a simple way to the final particle production. At Relativistic Heavy Ion Collider (RHIC) it has been estimated that  $\epsilon \sim 5$  GeV/fm<sup>3</sup>, well above the lattice QCD prediction ( $\epsilon_{\text{crit}} \sim 1$  GeV/fm<sup>3</sup> [10]) for the hadron gas to the QGP phase transition.

In this Letter, results on proton and antiproton production and baryon stopping in Au + Au collisions at  $\sqrt{s_{NN}} = 200$  GeV are presented. The data were collected with the BRAHMS detector at RHIC. The BRAHMS experiment consists of two independent spectrometer arms, the midrapidity spectrometer (MRS) and the forward spectrometer (FS), described in detail in [11]. The spectrometers consist of dipole magnets, time projection chambers (TPC), and drift chambers (DC) for tracking charged particles, and detectors for particle identification (PID). The MRS can be rotated  $30^\circ < \theta < 95^\circ$  and the FS  $2.3^\circ < \theta < 30^\circ$ , where  $\theta$  is the polar angle with respect to the beam axis. By combining different settings of angle and magnetic fields, (anti)proton transverse momentum spectra at different rapidities ( $0 \leq y \leq 3$ ) were obtained.

The interaction point (IP) is determined by the beam-beam counters (BB), with a precision of  $\sigma_{BB} = 0.7$  cm. The IP was required to be within 15 (20) cm of the nominal IP for the MRS (FS) analysis to minimize acceptance corrections.

Protons and antiprotons are identified using time of flight detectors (TOF) in the MRS (TOFW) and FS (H1 and H2), and by the Ring Imaging Cherenkov (RICH) in the FS. The TOF resolution is  $\sigma_{TOFW} = 80$  ps,  $\sigma_{H1} = \sigma_{H2} = 90$  ps. To identify (anti)protons it is required that the derived square of the mass,  $m^2$ , is within  $\pm 2\sigma$  of the proton  $m^2$  and at least  $2\sigma$  away from the  $m^2$  for kaons. This allows (anti)protons to be identified up to momentum  $p < 3.0$  GeV/c for TOFW,  $p < 4.5$  GeV/c for H1, and  $p < 6.5$  GeV/c for H2. The refractive index of the RICH,  $n = 1.0020$ , allows protons to be directly identified via a measurement of their ring radius in the range  $15 < p < 25$  GeV/c. By using the RICH to veto pions and kaons the PID can be extended down to  $p = 10$  GeV/c.

The collision centrality is determined using a multiplicity array located around the nominal IP [11]. In this analysis only the 0%–5% most central collisions were used. The mean number of participants for this centrality class was found by Glauber model calculations to be  $N_{part} = 357 \pm 8$  [12].

From the identified particles, the invariant differential yields  $\frac{1}{2\pi p_T} \frac{d^2N}{dy dp_T}$  were constructed for each spectrometer setting. The differential yields were corrected for geometrical acceptance, tracking and PID efficiency, absorption, and multiple scattering. The corrections for absorption and multiple scattering were less than 20% at the lowest  $p_T$  and less than 5% at the highest  $p_T$  in all settings. No corrections were applied for secondary protons from, e.g., the beam pipe, since the contribution was found to be negligible in GEANT based Monte Carlo (MC) simulations [13] using HIJING [14] as input, when the tracks were required to point back to the IP. The acceptance correction is purely geometrical and calculated using a MC simulation of the BRAHMS detector. The

tracking efficiency was estimated for the TPCs, by embedding simulated tracks in real events (method I), and in the FS where there are five tracking detectors (2 TPCs and 3 DCs) by comparing the number of identified track segments in the chamber to the number of reference tracks determined by other detectors disregarding the chamber under consideration (method II). In the front part of the FS (FFS) where both methods are applicable, there was a 10% discrepancy between the two methods that has been included in the systematic errors quoted below. For the spectrometers the total tracking efficiency depends on the spectrometer angle and is 90%–95% in the MRS, 80%–90% in the FFS (settings at  $y \sim 2$ ), and 60%–70% in the full FS ( $y \sim 2, y \sim 3$ ). The efficiencies of the TOF detectors were found to be 93%–98%. For the part of the spectrum at  $y \sim 3$ , where the RICH was used to veto pions and kaons a correction for contamination of pions and kaons with no identified ring radius was applied. The RICH inefficiency is 5%.

Figure 1 shows transverse momentum spectra for four of the nine measured rapidities. The net-proton spectra were constructed by subtracting the antiproton spectrum from the proton spectrum. At each rapidity, the proton, antiproton, and net-proton spectra have similar shapes, indicating that produced and transported protons have similar spectral properties. To obtain rapidity densities,

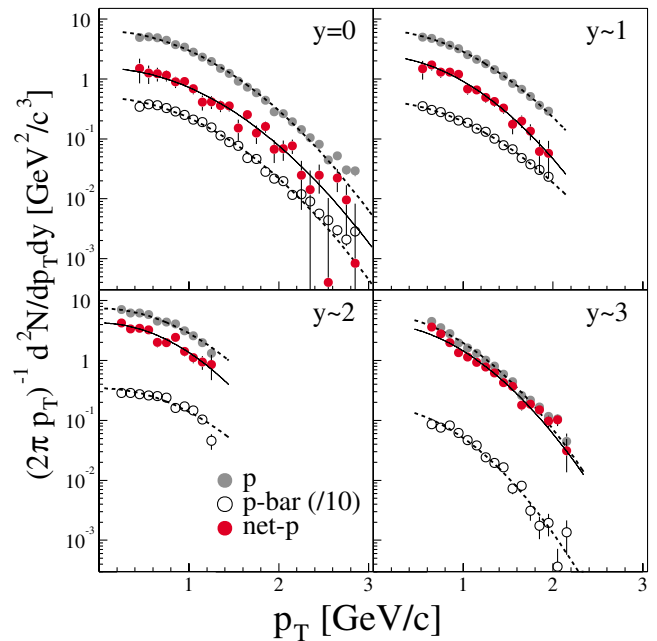


FIG. 1 (color online). Proton, antiproton, and net-proton transverse momentum spectra at selected rapidities,  $y \sim 0, 1, 2, 3$ . The solid and dashed lines represent Gaussian fits to the data (extended outside the fit range for clarity). The antiproton spectra have been divided by ten as indicated. The errors on the data points are statistical only, and no weak decay correction has been applied.

$dN/dy$ , for  $p$ ,  $\bar{p}$ , and net- $p$  their spectra are fitted, and the fit was used to extrapolate to the full  $p_T$  range. Different functional forms were tested:  $m_T$  exponential, Boltzmann, and Gaussian. The function found to best describe the data was the Gaussian in  $p_T$  [ $f(p_T) \propto e^{-p_T^2/(2\sigma^2)}$ ], and this function has been used for all fits. This functional form was also used in [15].

The mean transverse momentum  $\langle p_T \rangle$  of the spectra calculated from the fit is found to be within 0.1 GeV/ $c$  at each rapidity for the three functional forms. For protons that have the best counting statistics,  $\langle p_T \rangle$  decreases from  $\langle p_T \rangle = 1.01 \pm 0.01(\text{stat})$  GeV/ $c$  at  $y = 0$  to  $\langle p_T \rangle = 0.84 \pm 0.01(\text{stat})$  GeV/ $c$  at  $y \sim 3$ .

The differential yield within the measured  $p_T$  range varies from 85% of the total  $dN/dy$  near midrapidity to 45% at  $y \sim 3$ . The systematic errors on  $dN/dy$  were estimated from the difference in  $dN/dy$  values obtained using different spectrometer settings covering the same ( $y, p_T$ ) regions, from the discrepancy between the two different efficiency methods, and by estimating the effects of the  $p_T$  extrapolation. The systematic errors were found to be 10%–15% for midrapidity ( $y < 1$ ) and 20%–30% for forward rapidities.

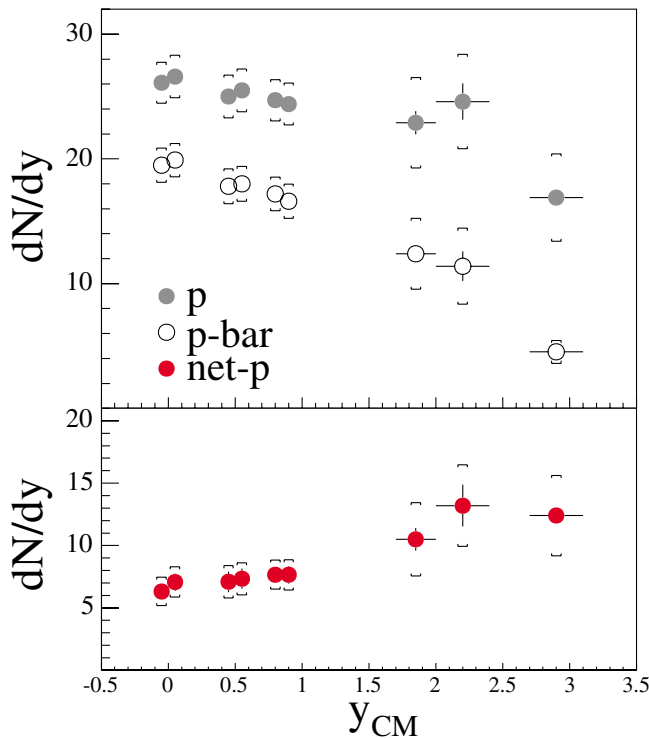


FIG. 2 (color online). Proton, antiproton, and net-proton rapidity densities  $dN/dy$  as a function of rapidity at  $\sqrt{s_{NN}} = 200$  GeV. The horizontal bars show the rapidity intervals for the projections. The errors shown with vertical lines are statistical only while the caps includes both statistical and systematic errors. No weak decay correction has been applied.

Figure 2 shows the resulting rapidity densities  $dN/dy$  as a function of rapidity. The most prominent feature of the data is that while the proton and antiproton  $dN/dy$  decrease at rapidities away from midrapidity the net-proton  $dN/dy$  increases over all three units of rapidity, from  $dN/dy(y = 0) = 6.4 \pm 0.4(\text{stat}) \pm 1.0(\text{syst})$  to  $dN/dy(y = 3) = 12.4 \pm 0.3(\text{stat}) \pm 3.2(\text{syst})$ .

A Gaussian fit to the antiproton  $dN/dy$  distribution gives the total extrapolated antiproton yield:  $84 \pm 6$  (92% in  $-3 < y < 3$ ). For protons the yield from a Gaussian fit to  $dN/dy$  in the range,  $-3 < y < 3$ , is  $138 \pm 7$ .

Figure 3 shows net-proton  $dN/dy$  measured at AGS and SPS compared to these results. The distributions show a strong energy dependence, the net protons peak at midrapidity at AGS, while at SPS a dip is observed in the middle of the distribution. At RHIC a broad minimum has developed spanning several units of rapidity, indicating that at RHIC energies collisions are quite transparent.

To calculate the rapidity loss,  $dN/dy$  must be known from midrapidity to projectile rapidity,  $y_p = 5.36$ . BRAHMS measures to  $y \sim 3$ , so the shape of the rapidity distribution must be extrapolated to calculate  $\langle \delta y \rangle$ . The baryon number of participating nucleons ( $N_{\text{part}}$ ) is conserved, while the net-proton number is not necessarily conserved. To obtain net baryons, the number of net

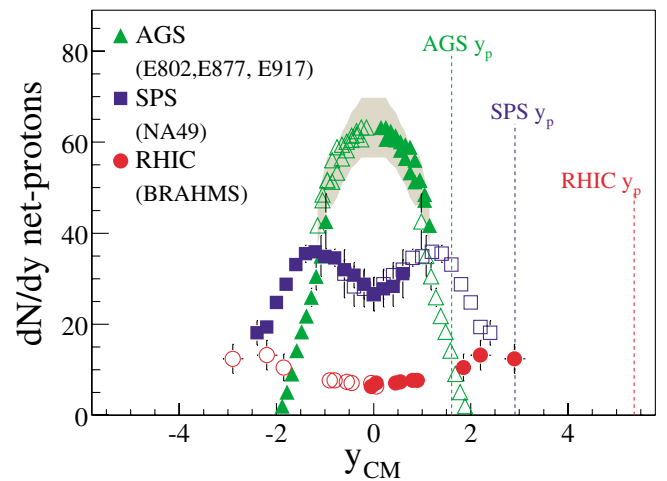


FIG. 3 (color online). The net-proton rapidity distribution at AGS [8,21,22] (Au + Au at  $\sqrt{s_{NN}} = 5$  GeV), SPS [23] (Pb + Pb at  $\sqrt{s_{NN}} = 17$  GeV), and this measurement ( $\sqrt{s_{NN}} = 200$  GeV). The data are all from the top 5% most central collisions and the errors are both statistical and systematic (the light gray band shows the 10% overall normalization uncertainty on the E802 points, but not the 15% for E917). The data have been symmetrized. For RHIC data black points are measured and gray points are symmetrized, while the opposite is true for AGS and SPS data (for clarity). At AGS weak decay corrections are negligible and at SPS they have been applied.

neutrons and net hyperons have to be estimated and the contribution from weak decays included in the measured net protons has to be deduced. Using MC simulations we find these contributions to be  $c_1 = 0.53 \pm 0.05$  protons for each  $\Lambda$ , and  $c_2 = 0.49 \pm 0.05$  protons for each  $\Sigma^+$  decay. There is a weak rapidity dependence which is included in the systematic error. The number of net-baryons is, then,

$$n_B = n_{p,\text{meas}} \frac{n_p + n_n + n_\Lambda + n_{\Sigma^+} + n_{\Sigma^-}}{n_p + c_1 n_\Lambda + c_2 n_{\Sigma^+}}, \quad (2)$$

where  $n_x = N_x - N_{\bar{x}}$  are the primary number of net neutrons ( $n_n$ ), net protons ( $n_p$ ), net lambdas ( $n_\Lambda$ ), and net sigmas ( $n_{\Sigma^-}$ ,  $n_{\Sigma^+}$ ), respectively, and  $n_{p,\text{meas}}$  is the measured net-proton yield. In addition to primaries, net lambdas,  $n_\Lambda$  includes contributions from other hyperons that decay to protons through  $\Lambda$ s, e.g.,  $\Sigma^0$ ,  $\Xi^0$ , and  $\Xi^-$ .

The ratio  $n_n/n_p = 1.00 \pm 0.05$  was found from HIJING [14] and AMPT [16] in the rapidity interval  $|y| < 3.5$ . The equilibration of protons and neutrons close to midrapidity has been experimentally observed at AGS energies [17].

At midrapidity the ratio  $N_\Lambda/N_p = 0.89 \pm 0.07(\text{stat}) \pm 0.21(\text{syst})$  was found to be equal within statistical errors to  $N_{\bar{\Lambda}}/N_{\bar{p}} = 0.95 \pm 0.09(\text{stat}) \pm 0.22(\text{syst})$  at  $\sqrt{s_{NN}} = 130$  GeV [18]. Those results indicate that  $N_\Lambda/N_p = N_{\bar{\Lambda}}/N_{\bar{p}} = n_\Lambda/n_p$ . We use  $n_\Lambda/n_p = 0.93 \pm 0.11(\text{stat}) \pm 0.25(\text{syst})$  at  $\sqrt{s_{NN}} = 200$  GeV and find at  $y = 0$  the number of feed-down corrected protons and antiprotons to be  $dN/dy = 17.5 \pm 1.2(\text{stat}) \pm 3.0(\text{syst})$  and  $dN/dy = 13.2 \pm 0.9(\text{stat}) \pm 2.3(\text{syst})$ , respectively, in agreement with the measurement at  $\sqrt{s_{NN}} = 200$  GeV by PHENIX:  $dN/dy(p) = 18.4 \pm 2.6(\text{syst})$  and  $dN/dy(\bar{p}) = 13.5 \pm 1.8(\text{syst})$  [19]. Assuming that  $n_\Lambda/n_p$  is constant over the full rapidity interval, the feed-down correction for  $\Lambda$  alone can be done as  $n_p = 0.67 \pm 0.12 n_{p,\text{meas}}$ . At forward rapidity  $\Lambda$ s have not been measured, and the conservative estimate  $n_\Lambda/n_p = 1.0 \pm 0.5$  is used.

The yields of  $\Sigma^+$  and  $\Sigma^-$  have not been measured at RHIC. In thermal models  $N_{\Sigma^+} \sim N_{\Sigma^-}$  and  $N_{\Sigma^-} \sim 0.1 N_p$  [20] at RHIC ( $\sqrt{s_{NN}} = 130$  GeV), and  $n_{\Sigma^+}/n_p = n_{\Sigma^-}/n_p = 0.10 \pm 0.05$  is used here.

The final correction is  $n_B = (2.03 \pm 0.08) n_{p,\text{meas}}$ . The systematic error on the final correction depends almost entirely on the error on  $n_n/n_p$  and  $n_{\Sigma^-}/n_p$  because the partial derivative of Eq. (2) with respect to  $n_\Lambda/n_p$  and  $n_{\Sigma^+}/n_p$  is very small for the numerical values used.

Figure 4 (inset) shows the net-baryon  $dN/dy$  obtained from the measured net-proton  $dN/dy$ . The net-baryon density in the rapidity region where BRAHMS has no acceptance can be constrained by the total integral, equal to  $N_{\text{part}}$ , and since diffractive scatterings can be ignored in central collisions where each nucleon on the average experiences several scatterings,  $dN/dy(y_p) \sim 0$ . To illus-

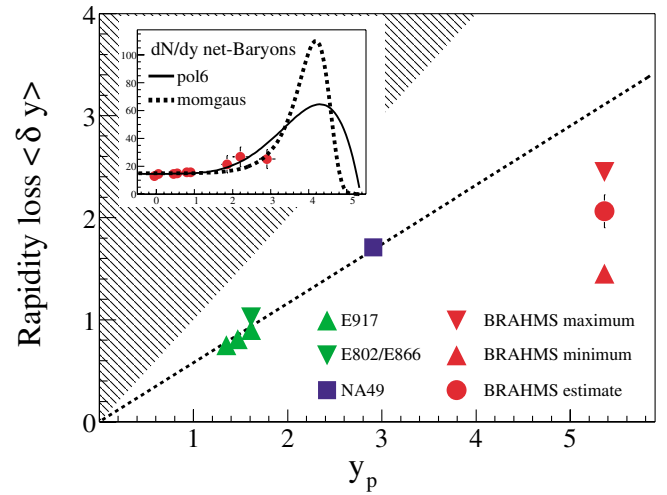


FIG. 4 (color online). The inset plot shows the extrapolated net-baryon distribution (data points) with fits (represented by the curves) to the data; see text for details. The full figure shows the rapidity loss, obtained using Eq. (1), as a function of projectile rapidity (in the CM). The hatched area indicates the unphysical region, and the dashed line shows the phenomenological scaling  $\langle \delta y \rangle = 0.58 y_p$ . The data from lower energy are from [6,8].

trate the extrapolation from the measured region,  $0 < y < 3$ , to beam rapidity,  $y_p$ , two different functions have been used: A six order symmetric polynomial (pol6)  $f(y)$  which is the simplest polynomial that describes the data points, has the correct integral, and  $f(y_p) = 0$ , and a Bjorken inspired symmetric sum of two Gaussians in momentum space (momgaus), converted to rapidity space using  $p = m \sinh(y)$  ( $p_T = 0$ ) where  $m$  is the proton mass. The momgaus gives a simple description of the data as the product of the two fragmenting nuclei with no midrapidity source. The data are consistent with Bjorken's picture of the collision where the fragmentation regions are far from midrapidity ( $y \sim 3-4$ ), but shows that there is still a significant number of baryons transported to midrapidity. From the momgaus fit a mean momentum of 31 GeV/c with a spread of 13 GeV/c is found. The rapidity loss is  $\langle \delta y \rangle = 2.04 \pm 0.10$  using the pol6 fit and  $\langle \delta y \rangle = 2.06 \pm 0.16$  for the momgaus fit, and the last value has been used as an estimate in Fig. 4. From the pol6 fit there are  $60 \pm 6$  net baryons in the rapidity interval,  $0 < y < 3$ , with a  $\langle \delta y \rangle = 3.60 \pm 0.05$ . If the remaining 118.5 net baryons are placed at  $y = 3.5$ , maximum  $\langle \delta y \rangle = 2.45$ , and  $y = 5.0$ , minimum  $\langle \delta y \rangle = 1.45$ , a conservative estimate for the possible range of values is obtained, also shown in Fig. 4. The rapidity loss at RHIC is clearly less than the phenomenological linear rapidity scaling would predict; this scaling is broken at RHIC.

Using the functional forms the total energy,  $E$ , per net baryon after the collision can be derived:

$$E = \frac{1}{N_{\text{part}}} \int_{-y_p}^{y_p} \langle m_T \rangle \cosh y \frac{dN_{B-\bar{B}}}{dy} dy. \quad (3)$$

The  $\langle m_T \rangle$  is known for protons from the spectra in the covered rapidity interval. Linear and Gaussian extrapolations of  $\langle m_T \rangle$  to projectile rapidity changes  $E$  by less than 5%. The energy is  $E = 30 \pm 2$  GeV for pol6 and  $E = 26 \pm 5$  GeV for the momgaus fits. Taking  $E = 27 \pm 6$ ,  $\Delta E = 73 \pm 6$  GeV of the initial 100 GeV per participant is available for excitations. Using the same minimum and maximum estimates above:  $47 < \Delta E < 85$  GeV.

In conclusion BRAHMS has measured proton, anti-proton, and net-proton yields from midrapidity ( $y = 0$ ) to forward rapidity ( $y \sim 3$ ). The net-proton distribution shows that collisions at RHIC energies are quite transparent compared to lower energies. By extrapolation to the full net-baryon distribution, we find that the rapidity loss scaling observed at lower energy is broken and the rapidity loss seems to saturate between SPS and RHIC energies.

This work was supported by the division of Nuclear Physics of the Office of Science of the U.S. DOE, the Danish Natural Science Research Council, the Research Council of Norway, the Polish State Committee for Scientific Research, and the Romanian Ministry of Research.

- 
- [1] S. A. Bass *et al.*, Nucl. Phys. **A661**, 205 (1999).
  - [2] S. Soff, J. Randrup, H. Stocker, and N. Xu, Phys. Lett. B **551**, 115 (2003).
  - [3] S. A. Bass, B. Muller, and D. K. Srivastava, Phys. Rev. Lett. **91**, 052302 (2003).

- [4] The rapidity  $y$  is defined as  $y = 0.5 \ln \frac{E+p_z}{E-p_z}$ . Rapidity variables are in the center-of-mass system with  $y_p$  positive.
- [5] W. Busza and A. S. Goldhaber, Phys. Lett. **139B**, 235 (1984).
- [6] F. Videbaek and O. Hansen, Phys. Rev. C **52**, 2684 (1995).
- [7] FOPI Collaboration, B. Hong *et al.*, Phys. Rev. C **57**, 244 (1998); **58**, 603 (1998).
- [8] E917 Collaboration, B. B. Back *et al.*, Phys. Rev. Lett. **86**, 1970 (2001).
- [9] J. D. Bjorken, Phys. Rev. D **27**, 140 (1983).
- [10] F. Karsch, Nucl. Phys. **A698**, 199 (2002).
- [11] BRAHMS Collaboration, M. Adamczyk *et al.*, Nucl. Instrum. Methods Phys. Res., Sect. A **499**, 437 (2003).
- [12] BRAHMS Collaboration, I. G. Bearden *et al.*, Phys. Rev. Lett. **88**, 202301 (2002).
- [13] GEANT 3.2.1, CERN program library.
- [14] X. N. Wang and M. Gyulassy, Phys. Rev. D **44**, 3501 (1991).
- [15] STAR Collaboration, C. Adler *et al.*, Phys. Rev. Lett. **87**, 262302 (2001).
- [16] B. Zhang, C. M. Ko, B. A. Li, and Z. w. Lin, Phys. Rev. C **61**, 067901 (2000).
- [17] K. N. Barish *et al.*, Phys. Rev. C **65**, 014904 (2002).
- [18] PHENIX Collaboration, K. Adcox *et al.*, Phys. Rev. Lett. **89**, 092302 (2002).
- [19] PHENIX Collaboration, S. S. Adler *et al.*, Phys. Rev. C **69**, 034909 (2004).
- [20] W. Broniowski and W. Florkowski, Phys. Rev. C **65**, 064905 (2002).
- [21] E802 Collaboration, L. Ahle *et al.*, Phys. Rev. C **60**, 064901 (1999).
- [22] E877 Collaboration, J. Barette *et al.*, Phys. Rev. C **62**, 024901 (2000).
- [23] NA49 Collaboration, H. Appelshauser *et al.*, Phys. Rev. Lett. **82**, 2471 (1999).